Experimental investigation on punching resistance of R-UHPFRC–RC composite slabs

Malena Bastien-Masse & Eugen Brühwiler

Materials and Structures

ISSN 1359-5997

Mater Struct
DOI 10.1617/s11527-015-0596-4

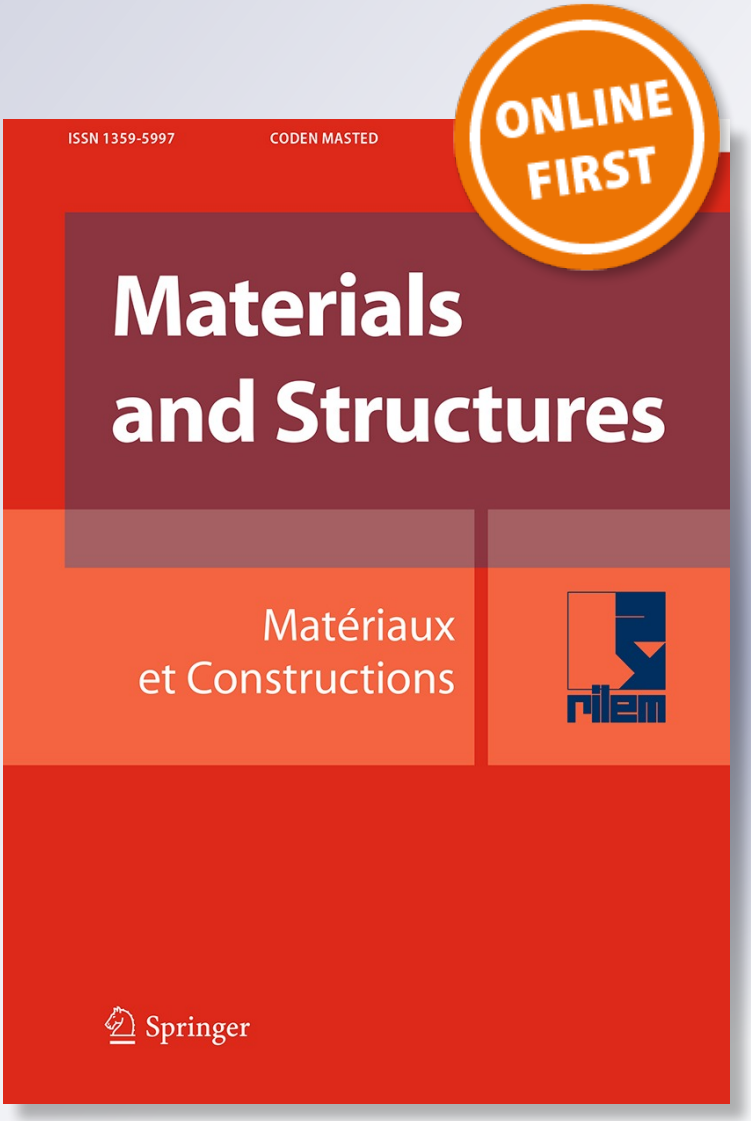

Springer

Materials and Structures
DOI 10.1617/s11527-015-0596-4

ORIGINAL ARTICLE

Experimental investigation on punching resistance of R-UHPFRC–RC composite slabs

Malena Bastien-Masse · Eugen Brühwiler

Received: 23 July 2014 / Accepted: 9 March 2015

Abstract An effective method to strengthen existing reinforced concrete (RC) structures is to add a thin layer of ultra-high performance fiber reinforced cement-based composite (UHPFRC), with or without steel rebars, over the concrete slab to create a composite element. It was demonstrated by previous test series that this method increases rigidity, bending and shear strength of one-way RC members. This paper presents the results of punching tests on six composite slabs without transverse reinforcement. The parameters of the tests included the thickness of the UHPFRC layer and the amount of reinforcement in it. All slabs failed in punching mode with a drop in resistance after the maximum resistance was measured. For a layer of 50 mm of UHPFRC, the normalised resistance was at least 1.69 times greater than the normalised resistance of the RC reference slab. The layer of UHPFRC increased the rigidity of the slab and provided added shear resistance to the cracked RC section by out of plane bending. By doing so, it allowed more deformation to take place in the RC section before punching failure. This results in rotations and deflections at maximum resistance similar to what was observed for the reference RC slab.

Keywords Composite slab · Punching shear · Ultra-high performance fiber reinforced cement-based composite (UHPFRC) · Strengthening · Near interface crack · Deformation capacity

List of symbols

Subscripts

R	Resistance
U	UHPFRC
c	Concrete
i	Steel or UHPFRC tensile reinforcement
sc	Top steel reinforcement layer in RC section
sU	Steel reinforcement in the R-UHPFRC layer

Latin upper case

A	Area
B	Side length of slab specimen
$E_{cm,28}$	Average modulus of elasticity of concrete at 28 days
$E_{Um,28}$	Average modulus of elasticity of UHPFRC at 28 days
V	Punching shear force
V_{csct}	Punching resistance of the concrete section calculated with CSCT
V_{flex}	Estimated flexural resistance calculated with yield lines

M. Bastien-Masse (✉) · E. Brühwiler
École Polytechnique Fédérale de Lausanne, Lausanne, Switzerland
e-mail: malena.bastien-masse@epfl.ch

E. Brühwiler
e-mail: eugen.bruehwiler@epfl.ch

Published online: 24 March 2015

V_{res} Residual shear resistance after punching failure

Latin lower case

b_0 Critical perimeter for punching shear set at $d_{sc}/2$ from the column face
c Side length of column
d Flexural depth for a tensile reinforcement: distance from the bottom compression face of the slab to the centroid of the tensile reinforcement
d_{eff} Effective flexural depth calculated with the mechanical ratio of each tensile reinforcement
d_g Maximum diameter of aggregate
d_{g0} Reference aggregate size set at 16 mm
f Strength of a material
f_c Concrete compressive strength,
$f_{cm,28}$ Average concrete compressive strength at 28 days
f_{sy} Yield strength of steel reinforcement
f_{su} Maximum strength of steel reinforcement
f_{Ute} Maximum tensile elastic strength of UHPFRC
f_{Utu} Maximum tensile strength of UHPFRC
h Height
Δh Change in thickness of a slab
Δl Change in distance between two points measured by a sensor
w Measured deflection of the slab; crack opening
Δw Shear deformation at the column face

Greek lower case

α_c Minimum angle of the critical shear crack
ε_{su} Strain in steel reinforcement at maximum strength
ε_{Utu} Strain in UHPFRC at maximum tensile strength
ψ Rotation
ω Mechanical ratio of tensile reinforcement
ω_{tot} Total mechanical ratio of tensile reinforcement

1 Introduction

Reinforced concrete (RC) flat slabs on columns are widely used in building construction for their simplicity to build. However, this type of construction has a basic conceptual flaw as it is prone to punching failure around the columns. This particular failure is known to be sudden and can trigger a progressive collapse of the structure [1].

To strengthen a RC slab with deficient resistance, it has been proposed to add on the surface a thin layer, 25–75 mm in thickness, of ultra-high performance fiber reinforced cement-based composite (UHPFRC) with small diameter steel rebars (Fig. 1a) [2]. This technique modifies the RC slab into an R-UHPFRC–RC (RU–RC) composite slab. The UHPFRC layer reinforced with steel rebar inserts (R-UHPFRC) acts as a tensile reinforcement and increases both bending and shear resistances of the slab.

UHPFRC is an ultra-high strength material with a very compact cement-based matrix. The high dosage in short straight steel fibers provides this material with outstanding tensile properties and ductility: tensile strength higher than 10 MPa with strain hardening and softening behavior (Fig. 1b) [3]. The addition of small diameter rebars to create an R-UHPFRC section improves the apparent UHPFRC tensile behavior by increasing the resistance and improving the deformation capacity and strain hardening behavior [4, 5].

The layer of R-UHPFRC is cast in place on the surface of the RC slab. The surface of the concrete must be adequately prepared prior to casting by high pressure water jetting or sand blasting in order to provide sufficient roughness. This ensures that the composite section will have a monolithic behavior in bending.

One-way RU–RC composite members were tested to study their behavior under bending and shear. Four point bending tests were carried out on composite beams and showed that the layer of UHPFRC significantly increases the bending resistance [5]. Moreover, no notable interface cracking was observed between the UHPFRC layer and the RC section prior to failure [6]. It is thus supposed that the behavior of composite beams is monolithic when submitted to pure bending moments and design can be done based on the plane-sections hypothesis. RU–RC composite beams were also tested in a cantilever test setup where they were submitted to high shear forces combined with bending [7]. These tests showed that the layer of UHPFRC also increases the shear resistance and deformation capacity of a RC beam.

The main goal of this new experimental campaign is to extend the knowledge from one-way to two-way RU–RC composite elements [8]. Focus is thus placed

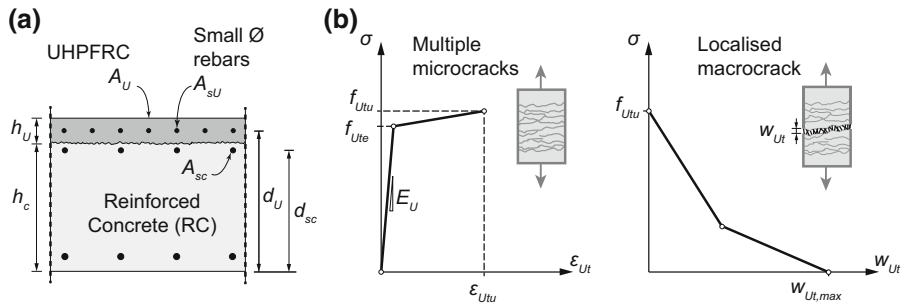

Fig. 1 **a** Typical RU–RC composite cross-section and notations [2], **b** constitutive law of UHPFRC [3]

on the behavior of RC slabs with no shear reinforcement submitted to concentrated forces with a layer of UHPFRC acting as a two-dimensional tensile reinforcement.

The tests were designed to study the contribution of the UHPFRC layer to two-way or punching shear resistance. The main parameter is the total amount of tensile reinforcement which was varied for each test in two ways:

(1) variation of the UHPFRC layer thickness;
(2) variation of the ratio of steel reinforcement in the UHPFRC layer.

Specimen size was also varied. No shear reinforcement was used and the ratio of reinforcement in the RC section was kept constant. The tests allowed studying deformation and cracking of the RC section and the UHPFRC layer and global rotation and displacements of the slab.

2 Background

2.1 Punching resistance of RC slabs without transverse reinforcement

In order to predict the resistance to punching of RU–RC composite slabs, mechanisms that govern the behavior of the RC section must be well understood. It will then be possible to study the influence of the UHPFRC layer on these mechanisms. Parameters that influence the punching resistance of a RC slab without transverse reinforcement are the ratio of longitudinal reinforcement and the concrete compressive and tensile strengths.

Punching is due to a vertical force acting perpendicularly to the slab, such as the force due to a column. It creates high shear forces that are first carried through an inclined compression strut connecting the concentrated force to the tensile reinforcement at an angle of 25°–30°. While deformations increase, the tensile strength of the concrete is reached and an inclined crack appears along this strut. This is normally observed at 50–70 % of the punching resistance of the slab [9]. Stress can still be carried by the crack due to residual tensile strength and aggregate interlock [1, 10, 11]. These mechanisms depend on the opening of the critical shear crack which is proportional to the rotation of the slab. Punching failure is sudden and followed by a drop in the resistance of the slab [12]. The failure surface has the shape of a truncated cone over the column. Delamination of the cover concrete is also observed.

Slabs with higher reinforcement ratio show higher punching resistance but smaller deformations [10]. The failure happens before any or limited yielding of the steel reinforcement. Guandalini et al. [9] showed that size also has an effect on the punching resistance of slabs. Normalized punching resistance increases with decreasing slab thickness, but the deformation capacity decreases.

2.2 Strengthening methods

Many methods to strengthen existing flat slabs have been developed to overcome deficient punching shear resistance: enlargement of the support area, post-installed shear reinforcement, prestressing or increasing the amount of flexural reinforcement [13]. This last method can be conducted by casting on the top face of the slab a new layer of reinforced concrete linked to the existing section with shear connectors [14]. It is also possible to cast a layer of UHPFRC directly on the prepared existing concrete surface without any mechanical connectors as proposed in this paper or to add externally bonded reinforcements made of steel or fiber-reinforced polymers (FRP).

The use of FRP sheets to increase punching resistance has been studied by various authors [15–18]. As expected, the slabs with added reinforcement have a stiffer behavior. The FRP sheet also delays and controls the development of inclined cracking in the RC slab. As expected for a slab with added flexural reinforcement, the punching resistance of the slab reinforced with FRP is higher but smaller deformations at maximum resistance and no yielding of the steel or the external reinforcement is noticed.

2.3 Shear resistance of RU–RC composite beams

A test series on RU–RC composite beams submitted to combined bending and shear was realised by Noshiravani and Brühwiler [7]. It showed that the RU–RC beams have a significantly higher stiffness than their RC reference beams alone and that the maximum resistance is increased by up to 2.77 times. These tests also demonstrated that, if designed adequately, an R-UHPFRC layer can prevent the shear failure expected for the RC beam alone.

If a flexure-shear failure occurs in a composite beam, it is first due to a vertical bending crack in the RC section that develops diagonally towards the support. The widening of this critical crack then creates a prying action on the UHPFRC layer which induces softening of the concrete volume below the interface, starting at the mouth of the crack (Fig. 2). This is known as the intermediate-crack induced debonding (ICD) [7] and it allows for a new failure mode. Over the ICD zone, the R-UHPFRC layer resists to the debonding action by bending in double curvature. The flexure-shear failure finally happens in a sudden manner due to the crushing of the concrete ahead of the incline crack. It is followed by a drop in the resistance of the beam. Nevertheless, most of the beams that failed in flexure-shear during this test series still reached their maximum bending resistance.

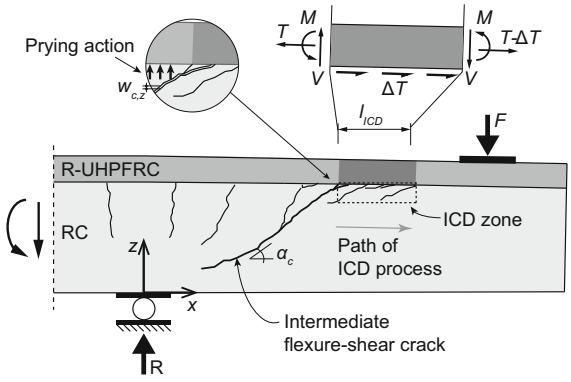

Fig. 2 Intermediate-crack induced debonding in RU–RC beams [7]

Since the R-UHPFRC layer increases the mechanical reinforcement ratio of the beam, it would be expected that the flexure-shear failure happens at a smaller deflection than the reference RC beam. However, as a result of the creation of the ICD zone, the deformation and rotation capacity of the composite beam is increased and the deflection at ultimate limit state is between 90 and 100 % of the reference beam.

The UHPFRC layer contributes in three ways to shear resistance of a composite beam. First, it hinders the widening of the critical shear crack. Second, it resists to the prying action by bending out of the plane. Third, the ICD zone modifies the stress fields in the beam and reduces the intensity of the shear stresses that must be carried across the critical shear crack. It is expected that the layer of UHPFRC will contribute to the punching resistance of two-way slabs with resisting mechanism similar to those observed for one-way shear resistance (Fig. 2).

3 Experimental investigations

3.1 Test specimens

A total of six square composite slabs were tested in punching over a column with a square cross section. Two different specimen sizes were used. All presented slabs had orthogonal reinforcement and a standard longitudinal reinforcement ratio in the RC section of 0.75 %. Table 1 gives the detailed parameters for each specimen.

In a first series called SAMD and tested by Wuest [19], two composite slabs of 200-mm total thickness and 2000-mm side lengths were tested. The thickness of the UHPFRC layer for the two SAMD slabs was respectively 50 and 25 mm, the thicker one being reinforced with high strength steel.

For the second series called PBM, four larger composite slabs were fabricated using similar dimensions as used by Guidotti [20] for tests on RC slabs: 260-mm total thickness and 3000-mm side lengths. Three of the composite PBM slabs had a 50-mm thick

Table 1 Main parameters of test series

Slab	Geometry				Steel in RC		Steel in UHPFRC		Effective reinf.	
	B (mm)	C (mm)	h_c (mm)	h_U (mm)	d_{sc} (mm)	Layout (mm)	Type	Layout (mm)	d_{eff} (mm)	ω_{tot} (%)
SAMD1[a]	2000	200	150	50	136	Ø14@150	High strength	Ø10@150	162	20.7
SAMD2[a]			172	23			–	–	153	8.9
PBM1	3000	260	210	50	180	Ø16@150	–	–	204	16.6
PBM2							Standard	Ø8@150	209	14.5
PBM3							High strength	Ø8@150	209	16.2
PBM4			235	25	210	Ø16@125	–	–	217	12.3
PG19[b]			250	–	210	Ø16@125	–	–	210	7.1
PG20[b]						Ø20@100				13.4

[a] Tested by Wuest [19]

[b] Tested by Guidotti [20]

layer of UHPFRC with a varying amount of reinforcement. The fourth slab had a thinner plain layer of only 25-mm thick.

For a composite slab, the effective flexural depth d_{eff} and total mechanical reinforcement ratio ω_{tot} are calculated with Eqs. 1 and 2 respectively where i stands for each layer of tensile reinforcement. As seen in Fig. 1a, the tensile reinforcement of a composite section includes the top steel rebars in the RC section (subscript sc), the layer of UHPFRC (subscript U) and the steel rebars in the UHPFRC layer (subscript sU).

$$d_{eff} = \frac{\sum d_i A_i f_i}{\sum A_i f_i} \quad (1)$$

$$\omega_{tot} = \sum \omega_i = \sum \frac{A_i f_i}{A_c f_c} \quad (2)$$

For every type of tensile reinforcement, d_i is the distance between the bottom compression face and the centroid of the layer of reinforcement (see notations in Fig. 1). A_i and f_i are the area per unit length and tensile strength (f_{sy} for rebars and f_{Utu} for UHPFRC). A_c and f_c are the area per unit length and compressive strength of concrete. All material strengths are given in Table 2.

All presented slabs also had layers of compression reinforcement at the bottom of the RC sections, with spacing as the top reinforcement. This reinforcement was made of Ø14-mm bars for slabs SAMD and of Ø10-mm for slabs PBM and PG19 and 20, the reference RC slabs.

The results of the PBM series were compared to chosen reference RC specimens PG19 and 20 tested by Guidotti [20]. All PBM slabs had an effective flexural depth d_{eff} close to 210 mm which is the flexural depth d_{sc} of PG19 and 20. These two slabs are part of a larger database of punching tests on RC slabs. Many slabs with the same dimensions, with or without shear reinforcement and with varying amount of flexural reinforcement have been tested under punching shear by various authors [9, 20–22]. Slabs PG19 and 20 have been chosen as being representative. Slab PG19 is the main reference slab because, as the RC sections of the composite slabs, it had a reinforcement ratio of 0.75 %. It also had the lowest mechanical reinforcement ratio ω_{tot} of all presented slabs. Slab PG20 had a higher reinforcement ratio of 1.50 %. It is interesting to compare its behavior to the case of composite slabs as it also had a higher mechanical reinforcement ratio, similar to the one of composite slab PBM4, 13.4 and 12.3 % respectively.

3.2 Material properties

The RC section of all specimens was fabricated with conventional concrete with a maximum aggregate diameter of 16 mm. The age of the concrete when the specimens were tested is given in Table 2 as well as the average concrete properties at 28 days obtained from standardized tests on three cylinders.

The UHPFRC layer of SAMD series was made with mix CM22 which contained 10-mm long straight steel fibres and steel wool. This CM22 mix is part of the CEMTEC$_{multiscale}$© family of UHPFRCs developed by Rossi [23, 24] and adapted for rehabilitation. The

Table 2 Tested material properties

Concrete			
Slab	Age at testing (days)	$E_{cm,28}$ (GPa)	$f_{cm,28}$ (MPa)
SAMD1[a]	192	33.3	51.4
SAMD2[a]	176	34.2	46.7
PBM1	114	25.5	32.6
PBM2	101	27.7	36
PBM3	88	25.5	32.3
PBM4	76		
PG19[b]	20	32.7	46.2
PG20[b]	33	33.9	51.7

UHPFRC				
Type	Elastic		Strain hardening	
	$E_{Um,28}$ (GPa)	f_{Ute} (MPa)	ε_{Utu} (‰)	f_{Utu} (MPa)
CM22[a]	47.2	11.2	1.4	13.3
S3-13	44.5	6.6	1.2	7.5

Steel					
Type	$\emptyset$ (mm)	f_{sy} (MPa)	f_{su} (MPa)	f_{su}/f_{sy}	ε_{su} (%)
High strength	8	772	905	1.17	2.9
	10[a]	937	959	1.02	Not measured
Standard	8	532	606	1.14	5.7
	10	518	616	1.19	6.7
	14[a]	526	607	1.15	Not measured
	16	546	621	1.13	11.9
	20[b]	551	659	1.20	9.4

[a] Material properties obtained from Wuest [19]

[b] Material properties obtained from Guidotti [20]

tensile properties of UHPFRC CM22 given in Table 2 are the average of three tests on individually cast specimens [19].

For the PBM series, the UHPFRC layer was fabricated with an industrial premix named S3-13 containing 13-mm long straight steel fibers. This material was submitted to an extensive characterization campaign. To obtain its tensile properties, 16 dog-bone shaped specimens were cut out from four square plates of 50-mm thick and 1000-mm sides. This fabrication method allowed capturing the variability of tensile behavior in a plate similar to the layers cast on the composite slabs. The tensile properties of UHPFRC S3-13 given in Table 1 are the average of 11 tests on these dog-bone specimens.

The UHPFRC layers were cast on a washed concrete surface with exposed aggregates. The layer was applied from one side of the slab progressing towards the other. It is reasonable to assume that this procedure slightly oriented the fibers in the casting direction.

The RC section of all slabs was fabricated using standard hot rolled steel rebars with nominal yield strength of 500 MPa. The same type of steel was used in the UHPFRC layer of slab PBM2. For slabs SAMD1 and PBM3 however, high strength steel with yield strength higher than 750 MPa was used in the UHPFRC layer. The steel properties in Table 2 are the average values from standardized tensile tests on three random samples.

3.3 Test setup and procedure

All specimens were tested in a 9-point system (Fig. 3), with the column in the center and 8 loading points located on a circle around it. The tests were displacement controlled at constant rates using hydraulic systems. Loading was stopped at planned force levels during the tests in order to make some observations and manual measurements.

The PBM slabs were tested in the setup developed for RC slabs by Guandalini et al. [9] and also used by Guidotti [20] for the RC slabs PG19 and 20 (Fig. 3a). The layer of UHPFRC was placed on top and the concrete face was resting on a square 260-mm side length column. The force was applied downwards in 8 points with a system of rods and hydraulic jacks placed bellow the laboratory strong floor. The eight steel loading plates were squares of 200-mm side length. These loading points were placed on a circle of 1500-mm radius. For these slabs, self-weight and weight of the test setup was added to the measured force.

The SAMD slabs were tested upside down, with the UHPFRC layer at the bottom (Fig. 3b). It was resting on eight rollers with square steel plates of 100-mm side length. These supports were placed on a circle of 1000-mm radius. The force was applied downwards with a hydraulic jack on the top concrete face. The square loading plate had 200-mm side length.

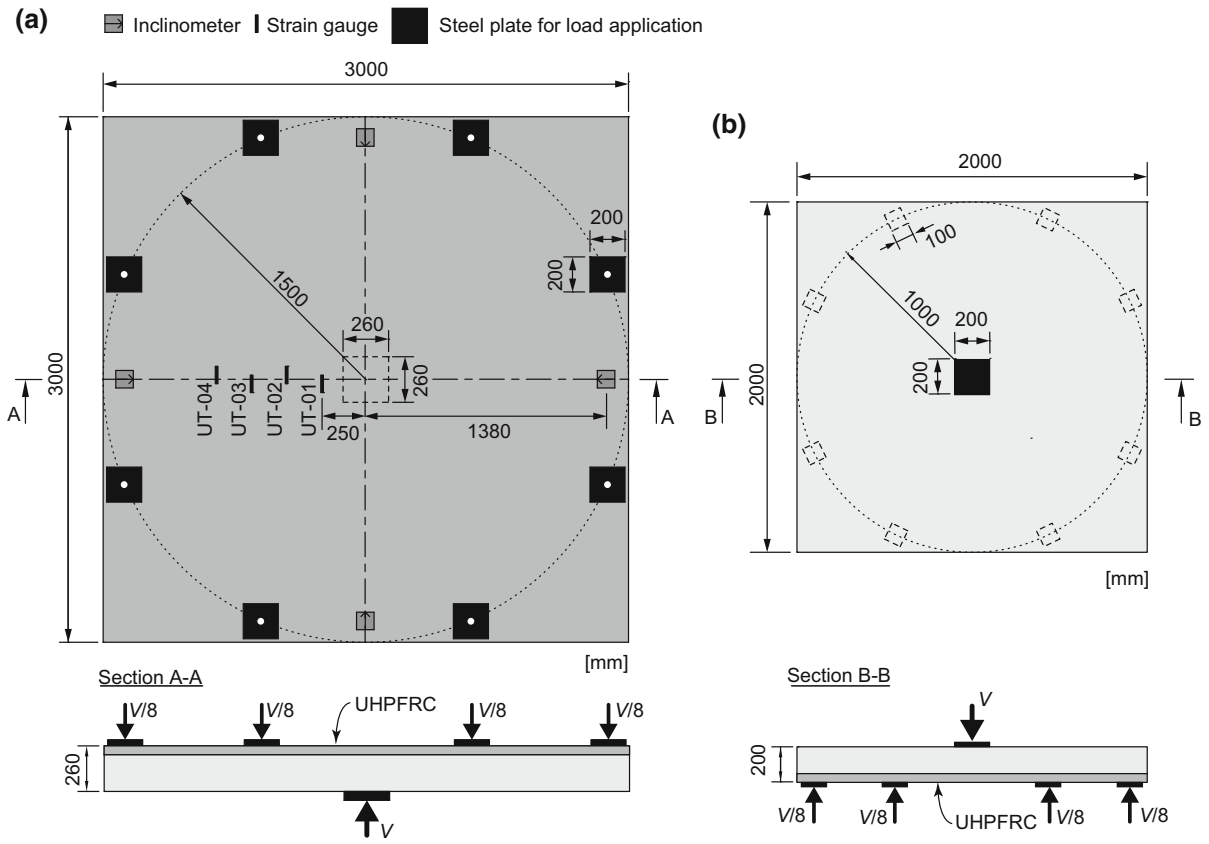

Fig. 3 Schematic test setup: **a** PBM series, **b** SAMD series [19]

In the following, and for simplicity, all slabs will be described as if they had been tested in a normal position for a composite slab, with the UHPFRC layer on top.

Continuous measurements were made during the tests. Load cells were placed at the hydraulic jacks to monitor the acting force. Strain gauges with 100-mm base lengths were placed on the UHPFRC and concrete faces. With reference to the laboratory strong floor, vertical deflections were measured at various points from the top and bottom sides of the slabs.

For the PBM series, rotation was recorded using inclinometers arranged on a 1380-mm radius circle (Fig. 3a). Local thickness variation in the slab was also measured. It corresponds to the vertical relative displacements of the top and bottom face of the slab. The device used to record the change in thickness has been described by Lips et al. [22] and Clément et al. [21].

4 Experimental results and discussion

4.1 Force—rotation response and failure mode

All normalized force—rotation curves are given in Fig. 4. The curves are normalized to neutralize the effects of various concrete compressive strengths and specimen and column sizes. In the case of the SAMD slabs, the rotations were not measured. They were approximated using the deflection measurements made below the loading point and supposing that the center of rotation is at the column face.

All slabs failed in punching mode. The failure is defined by the instant when the resistance drops suddenly after the maximum force is recorded. The plots in Fig. 4 show the slab response up to the maximal resistance before this resistance drop. The last reading before this drop is represented by a circle. The small drops in the force—rotation curves are due to the planned pauses in the tests. PBM3 was partially

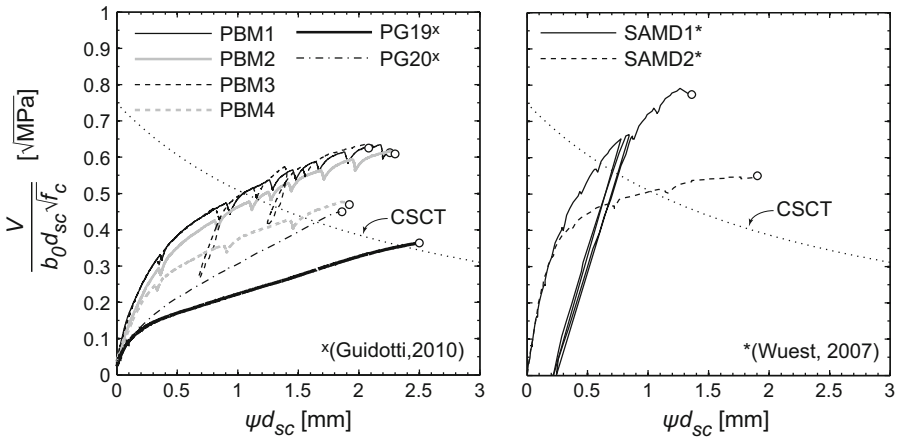

Fig. 4 Normalized force—rotation curves

unloaded twice and SAMD1 was completely unloaded twice. The slabs were unloaded to record any stiffness change.

Tests on slabs PBM1 and 2 and PG19 and 20 were ended right after the drop in resistance due to punching failure. In the other cases, the displacement increase was continued after the punching failure in order to record the post-peak behavior. This post-peak behavior will be discussed later in this paper.

Table 3 gives an overview of the main results for each slab: the maximum resistance (V_R), the rotation and deflection at V_R (ψ_R and w_R), the residual resistance (V_{res}) after the resistance drop and the minimum angle of the punching cone (α_c) measured on the cracking pattern (Fig. 5).

The ratio between the normalized maximum resistance of slabs PBM and the reference slab PG19 (Table 3) shows that the increase in resistance is between 69 and 75 % for a slab with a layer of 50 mm of UHPFRC (PBM1-3) while the increase is of 31 % for a 25-mm layer (PBM4). In all cases, this increase in resistance is significant.

Although it is expected that the addition of tensile reinforcement would reduce the rotation capacity while increasing the punching resistance of the slab, this was not observed for PBM1-3, which all had a 50-mm layer of UHPFRC. These three slabs failed at rotations close to what was measured for PG19, between 11.3 and 12.2 ‰. The composite slabs PBM1-3 all had approximately the same normalized resistance which indicates that failure occurred before yielding of the tensile reinforcement in the UHPFRC layer of slabs PBM2 and 3. The use of an R-UHPFRC layer for the specific case of punching reinforcement is

Table 3 Main test results

Slab	α_c (°)	V_R (kN)	V_R/V_{PG19} (–)	Normalised ratio $V_{Rnorm}/V_{PG19norm}$ (–)	ψ_R (‰)	w_R (mm)	V_{res} (kN)	V_{res}/V_R (–)
SAMD1[b]	20	971	–	–	9.6[a]	8.6	480	0.49
SAMD2[b]	23	675	–	–	13.4[a]	12.1	236	0.35
PBM1	24	1089	1.27	1.74	11.9	14.0	335	0.31
PBM2	28	1223	1.42	1.69	12.2	14.8	365	0.30
PBM3	21	1186	1.38	1.75	11.3	13.2	308	0.26
PBM4	29	1023	1.19	1.31	9.1	10.2	249	0.24
PG19[c]	22	860	1.00	1.00	12.1	13.7	–	–
PG20[c]	25	1094	1.27	1.24	9.2	10.9	–	–

[a] Calculated

[b] Tested by Wuest [19]

[c] Tested by Guidotti [20]

thus not necessary, as a plain layer of UHPFRC with the same thickness brings the same gains in resistance and deformability.

In the case of slab PBM4 which had a UHPFRC layer of 25-mm thick only, the resistance was also increased, but the rotation reduced compared to PG19. Slab PBM4 had a maximum resistance and rotation closer to what were measured for RC slab PG20, which has a higher reinforcement ratio than PG19. However, the force—rotation curves (Fig. 4) show that the composite slab PBM4 has a higher rigidity than slab PG20.

Finally, SAMD1, with a 50-mm layer of UHPFRC reinforced with a large amount of high strength steel, failed at a measured deflection lower than what was measured for SAMD2 which was reinforced with only a 25-mm layer of UHPFRC.

4.2 Cracking patterns

The slabs were cut on their central axis after the tests were ended and the internal cracking patterns could then be observed on the cut sections (Fig. 5). Figures 5 and 6 show the fully developed cracking patterns of, respectively, the cut face and the top tensile surface. The figures also indicate, for the composite slabs, at which load and displacement the test was ended. Because all tests were stopped at different levels of deformation, the patterns show differences in crack opening and extent of cracking. The cracking patterns seen for slabs PBM1 and 2 and PG19 and 20 reflect the cracking state right after the resistance drop due to the punching failure.

All punching cones observed on the cut slabs in Fig. 5, including the reference RC slabs PG19 and 20, have a similar shape with an angle α_c between 20° and 30° with respect to the horizontal (Table 3). The layer of UHPFRC does not appear to significantly modify the inclination of the critical shear crack in the lower part of the concrete. In the composite slabs, this main critical diagonal crack rotates just below the interface between the concrete and the UHPFRC layer, at the level of the upper rebar layer in the concrete. The failure of the concrete and not of the clear interface proves that the bond between the UHPFRC layer and the RC section is sufficient.

No significant vertical bending cracking is observed over the column in the RC sections of the composite slabs contrary to PG19 (Fig. 5). However, between one and three vertical cracks are visible in the UHPFRC, with typical crack mouth opening at maximum resistance of 0.5–0.7 mm for slabs PBM1-3, as measured by the strain gauges of 100-mm base length. These openings show that the UHPFRC is softening in this location, meaning that the measured strains are higher than the strain at maximum tensile strength (ε_{Utu}). These vertical cracks in the UHPFRC layer are accompanied by limited horizontal cracking in the concrete, near the interface.

Figure 6 gives indications on how the layer of UHPFRC contributes to the resistance of the slab. In the case of the slabs with a 50-mm layer (SAMD1, PBM1-3), a large number of radial cracks are visible which supposes that a thicker layer mainly contributes to the resistance by a tangential bending mechanism. In the case of the slabs with a thin layer of 25 mm (SAMD2, PBM4), radial cracking is limited and circular cracking is observed. The behavior of this thin layer is likely to be more governed by the radial bending moment around the head of the truncated punching cone.

4.3 Deflections, deformations and strains

4.3.1 Thickness variation and UHPFRC cracking

The thickness variation measurements give indications on how the cracking developed inside the slab. The exact locations of those measurements are shown in Fig. 5. Two measurements were taken close to the column (Ep01 and Ep02). These measurements showed that internal cracking for composite slabs started at 50–70 % of the maximum punching force V_R (Fig. 7), which is similar to what had been previously observed for RC slabs [9, 11]. Yet, it is clear in Fig. 7 that, up to maximum resistance, the layer of UHPFRC of the composite slab allowed the cracking in the concrete to develop much more then what was observed for the RC slab PG19. At maximum resistance, for all the composite slabs, the thickness of the slabs had increased by 1–1.5 mm (measured near the column by Ep01). For PG19, this increase was 3–5 times less. It is interesting to note that PBM4, which had a thinner layer of 25 mm of UHPFRC, allowed as much crack development inside the slab as for the slabs with a layer of 50 mm.

The opening of radial cracks on the top surface of the UHPFRC layer was captured by the strain gauges. Strain gauge UT01 (Fig. 3) was placed at 250 mm

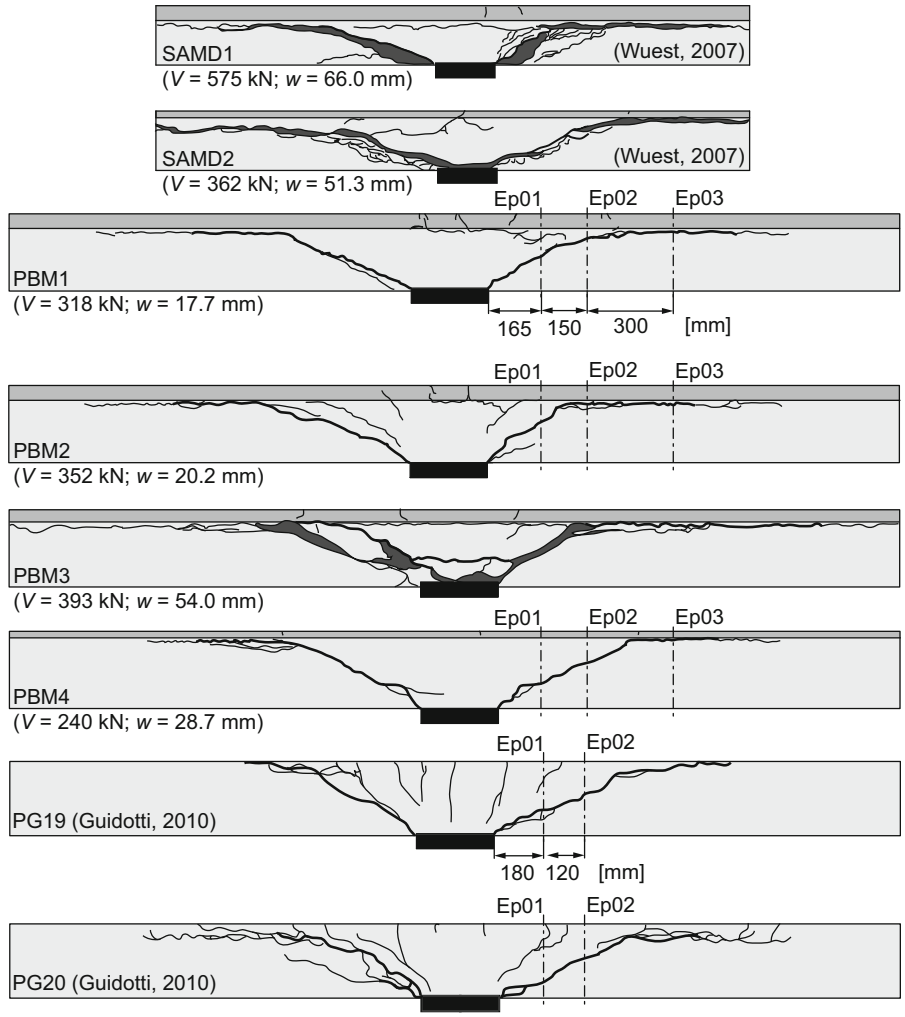

Fig. 5 Fully developed cracking pattern on cut sections of the slabs at the end of the test and position of the thickness measurements

from the center of the slab and measured radial displacements over a 100-mm base length. The measurements of UT01 showed that radial cracks also started localizing approximately at the same instant as the internal cracking started developing (Fig. 7). A crack has localized when the measured strain is higher than the strain at the maximum tensile strength of the UHPFRC (ε_{Utu}), meaning that the material has started softening at the measured location.

For the composite slabs PBM, a third measurement (Ep03) was taken further away from the column face. At this location, cracking in the concrete near the interface with the UHPFRC layer can be observed in the fully developed crack pattern (Fig. 5). However, no change in the thickness was recorded at this location prior to the punching failure which reveals that near interface cracking had not yet propagated that far. Near interface cracking observed on the cut sections (Fig. 5) thus developed after the punching failure when the relative displacement between the punching cone and the outside part of the slab became more important. The layer of UHPFRC could not be punched by the top of the concrete cone and the critical shear crack in the concrete had to rotate to become parallel to the interface.

4.3.2 Slab deformation

The top and bottom deformed shape of composite slab PBM1 and reference RC slab PG19 are compared in

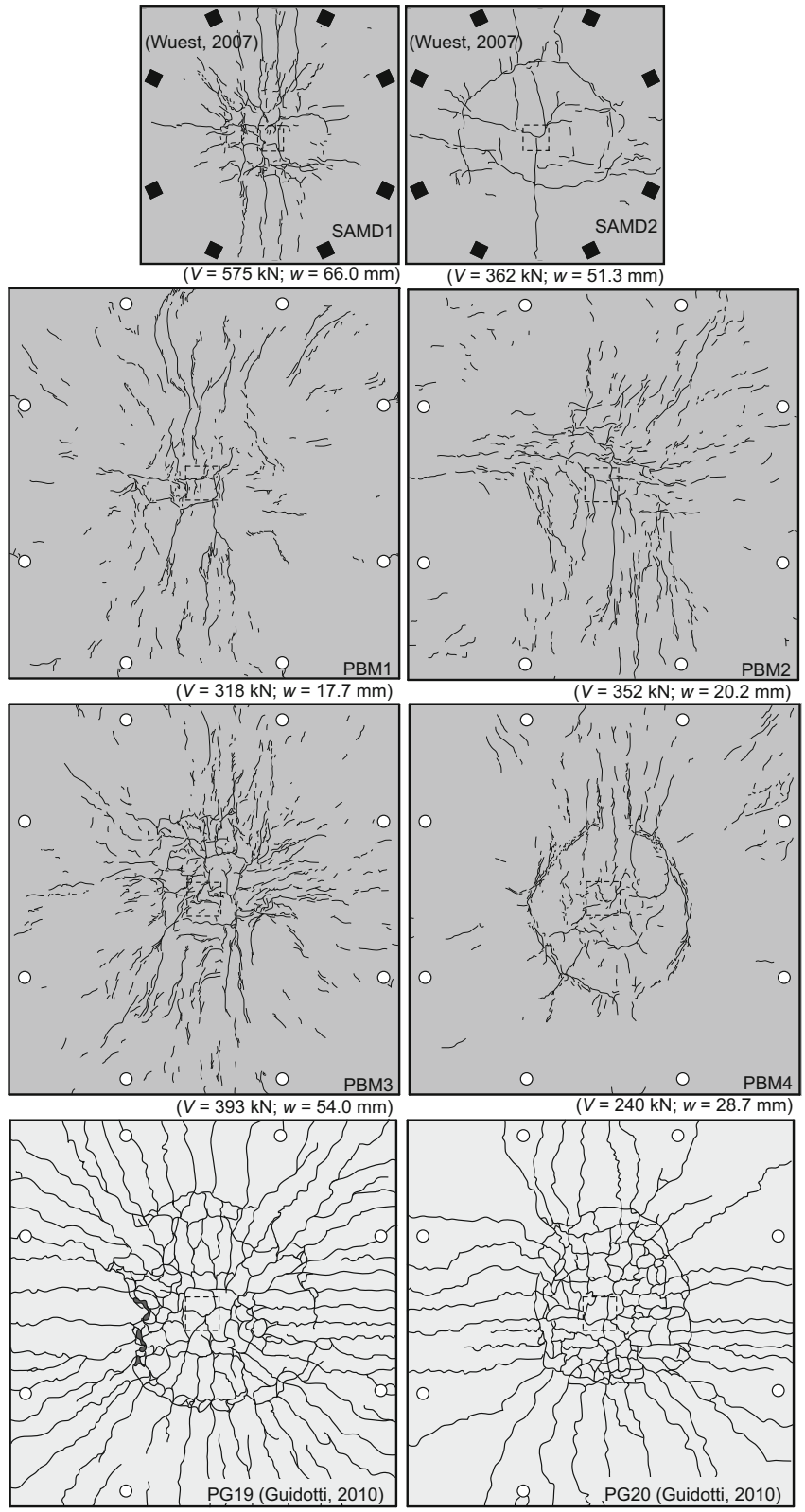

Fig. 6 Fully developed cracking pattern of the top tensile faces at the end of the tests

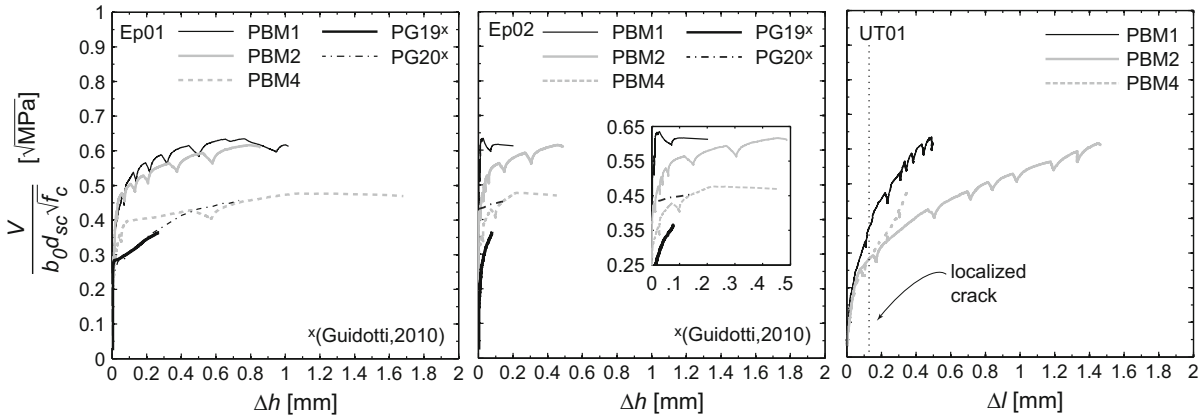

Fig. 7 Change of thickness of the slab in two locations (Ep01 and 02) and radial displacements of the UHPFRC layer (UT01) as a function of the normalized force

Fig. 8. The two slabs had approximately the same maximum deflection at maximum resistance, which is consistent with what was observed for rotations.

In both cases, the bottom face of the slab rotated around the column face with an increase in the rate of deflections after 60 % of the maximum force V_R, which corresponds to the start of the development of internal cracking (Fig. 7). For the RC slab PG19, this increase in the rate of deflections also appeared on the top face at a distance from the column face equal to the flexural depth of the slab (d_{sc}). This reflects the rigid body movement of the sector located outside the critical shear crack necessary to activate shear resistance once the concrete is cracked [20].

This rigid body movement was also observed in the composite slab PBM1 after internal cracking started to develop but it was accompanied by an upward deflection of the UHPFRC layer. Over the column and up to a distance of d_{sc} from the column face, the top surface lifted up instead of stabilizing at a constant position as for the RC slab.

This upward movement of the top surface in the composite slab is also illustrated by the plots in Fig. 8b showing together, as a function of the normalized force, the top deflections (IS3) and bottom deflections (II3) both located at the same horizontal distance from the column face. The difference between these two measurements is illustrated by the shaded area on the graphs. For both slabs, top and bottom face had the same rate of deflection up to 50–70 % of the maximum force V_R when, as showed before, internal cracking started to develop inside the RC section. Then, in the case of PG19, the rate of deflection of the top surface (IS3) reduced when compared to what was measured on the bottom face (II3). For the composite slab PBM1, the rate of deflection measured on top was reduced and then inversed. From 88 % of V_R the top face of PBM1 had an upward movement, while the bottom face continued its downward movement. At maximum resistance, the difference between top and bottom surface was 1.5 mm. A part of this difference can be attributed to the thickness variation due to the development of internal cracking in the slab but this cannot be more than 0.7 mm for PBM1 (Fig. 7). The rest of the difference corresponds to the upward deflection of the top surface.

The deflection measured on the top surface directly over the column (IS1) also reflects the upward movement, as seen in Fig. 8b. If the settlement of the column support plate is taken into account (measured by IIc1 and c2, in Fig. 8), the upward deflection of the top face of the slab over the column was of 0.8 mm at maximum resistance.

4.3.3 Shear deformation

Shear deformation at the column face Δw, illustrated in Fig. 9, is calculated with Eq. 3 using the deflection measurements made under the slab [22]. It is the relative displacement between the cone and the slab sector located outside the critical shear crack.

$$\Delta w = (w_{12} - w_{c2}) - \frac{(w_{12} - w_3)}{x_0} \cdot x_1 \qquad (3)$$

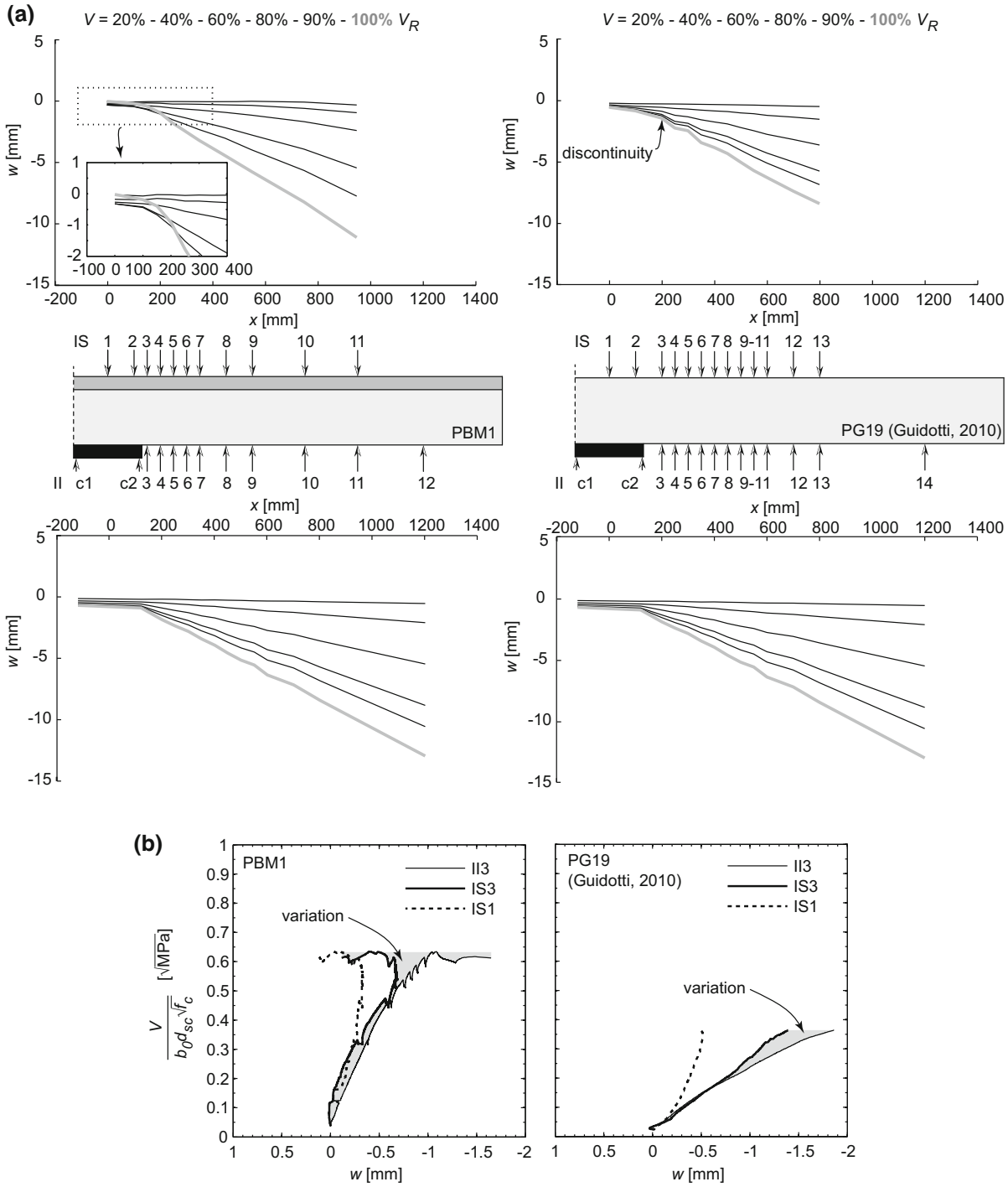

Fig. 8 Deflections of the PBM1 and PG19: **a** top and bottom deformed shapes, **b** central deflections as a function of the normalized force

Shear deformation as a function of the normalized force is plotted in Fig. 9. The RC slab PG19 had very limited shear deformation prior to maximum resistance, lower than 0.1 mm. In the case of the composite slabs, shear deformation was 3 to 8 times higher depending on the thickness of the layer of UHPFRC.

4.3.4 Concrete strains

Strains on the concrete bottom face of the slab were measured tangentially at 100 mm from the column for slabs PBM and PG19 and 20. For the RC slabs PG19 and 20, compressive strains reached values of 2 ‰ just prior to the punching failure. For the composite slabs with a 50-mm layer of UHPFRC (PBM1-3), the measured values were two times bigger, reaching compressive strains of 4 ‰. This is just another demonstration of the increase in deformability of the RC section provided by the addition of the UHPFRC layer.

4.4 Contribution of the UHPFRC layer to punching resistance

From the previous observations made with the experimental results, it is clear that the layer of UHPFRC increases rigidity and maximum punching resistance of a RC slab while keeping the rotation capacity equivalent. Due to the bending moment applied on the composite slab, the UHPFRC layer primarily contributes to the bending rigidity of the composite slabs by carrying tensile stress.

However, because of the movements in the RC section, the UHPFRC layer is also subjected to bending efforts over the column as shown by the development of vertical bending cracks in the layer over the column. These cracks are also observed on the surface of the layer, progressing radially from the center of the slab.

When internal cracking starts to develop in the RC section, at 50–70 % of the maximal force V_R, one to three vertical cracks localize in the UHPFRC layer over the column creating plastic hinges. Shortly after, at about 85 % of V_R, the layer of UHPFRC deflects upwards due to the rotation in the hinges.

The RC section cannot follow the upward deflection of the UHPFRC layer and limited near interface cracking develops to ensure geometrical compatibility. Very limited near interface cracking is also assumed to develop in the concrete at the mouth of the critical shear crack. This inclined critical crack cannot propagate through the layer of UHPFRC. Instead, bending efforts are introduced in the UHPFRC layer by the relative movement between the two lips of the critical shear crack, creating this second zone of near interface cracking. Figure 10 illustrates the assumed cracking state in the composite slab at maximum resistance.

Thus, the layer of UHPFRC carries part of the shear force by bending. By doing so, it allows more deformation to take place in the RC section before punching failure. This has been demonstrated by various measurements taken around the column: thickness variation, which reflects the development of cracking in the RC section, shear deformation at the column face and compressive strain at the soffit of the slab. This increased deformation of the RC section explains why the rotation capacity of the composite slab is larger than what is expected for a slab with an added flexural reinforcement. The development of cracking and the opening of the critical crack also have an influence on the punching shear resistance of the RC section.

In the case of slab SAMD1, the layer of UHPFRC was heavily reinforced. This made the layer stiffer and reduced its deformation capacity in bending. As a result, the global rotation of this slab was lower at maximum resistance than what was measured for SAMD2 with a thinner layer of UHPFRC.

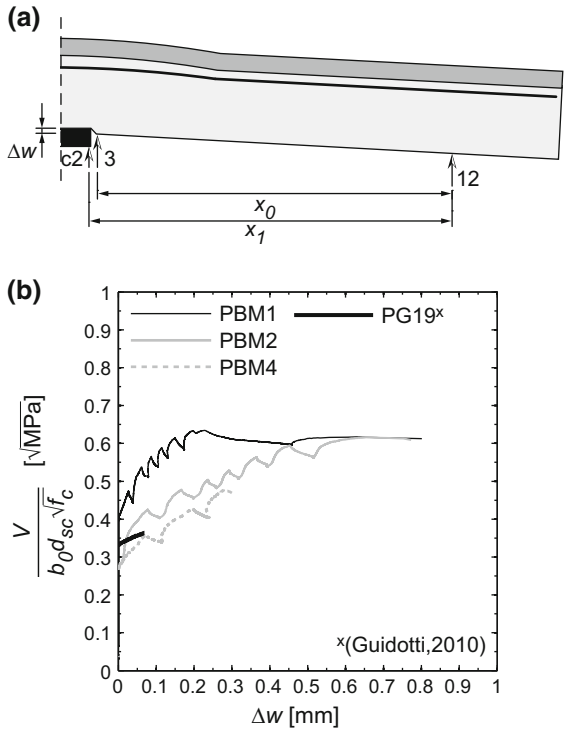

Fig. 9 **a** Definition of shear deformation [22], **b** shear deformations at column face as a function of the normalized force for selected specimen

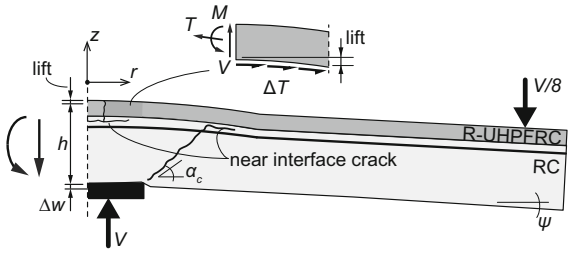

Fig. 10 Bending of the UHPFRC layer and shear deformations at column face

A thinner layer of 25 mm of UHPFRC can also increase the maximum resistance of a slab by over 30 %, depending on the ratio between the thickness of the UHPFRC layer and the thickness of the RC section. It will also carry shear by bending and allow more deformation to take place in the RC section. However, the bending effort introduced by the opening of the critical shear crack overpasses the bending moment of the thin layer and circular cracking develops in the layer near the mouth of the inclined crack before any extensive radial cracking (Fig. 6). The bending resistance of the layer being smaller, less shear can be carried and the failure will finally happen for a smaller rotation than for the RC reference slab.

4.5 Post-peak remaining resistance

The residual resistance of the composite slabs right after the punching failure was between 49 and 24 % of the maximum resistance (Table 3). It corresponds to the carrying capacity of the UHPFRC layer and the top reinforcement in the RC section. These elements provide shear support by bending of the UHPFRC layer and dowel action of the rebars. SAMD1 has a larger post-peak resistance due to the high amount of reinforcement in the UHPFRC layer.

The post-peak behavior was only measured for selected slabs and is shown in Fig. 11. In the case of slabs PBM, the deflection measurements in post-peak is recorded with II12 located at 1200 mm from the center of the slab (see position in Fig. 8). For slabs SAMD, the defection is measured right below the loading point, at the center of the slab.

As was shown by Fernández et al. [25], post-peak resistance due to flexural reinforcement, such as the UHPFRC layer and the top tensile rebars, is activated right after punching failure and remains stable when the displacement is increased. The increase in post-peak resistance in Fig. 11 is due to the bottom compression rebars passing above the column, as also observed by the aforementioned authors and by Habibi et al. [26]. Due to this, when the tests were ended, post-peak resistance had reached values up to 60 % of the maximum resistance.

Near interface cracking in the concrete also continues progressing in the post-peak regime as the relative displacement between the punching cone and the outside sector of the slab increases. This horizontal cracking is expected to stop in the regions where clamping is provided such as support areas or at the point of zero moments in the case of a continuous slab.

This residual post-peak resistance is not of interest for resistance based design; however it enhances the robustness of structures by avoiding progressive collapse of flat slabs [25, 26].

5 Comparison with resistance models for RC slabs

5.1 Overview

In the following, resistance models for RC slabs are used to emphasis the contribution of the UHPFRC layer to the punching resistance of a RC section. The yield-line method is used to calculate the bending resistance and the Critical Shear Crack Theory (CSCT) [10] is used to calculate the punching resistance of the RC section of the composite slabs.

5.2 Yield-line method

The bending resistance (V_{flex}) of each slab, given in Table 4, is estimated using the yield-line method, as was proposed by Guandalini et al. [9]. As expected, punching failure always happens before the slab reaches its maximum bending resistance. For the slabs with more reinforcement, such as the composite slabs with a 50-mm layer (SAMD1, PBM1-3), the punching failure happened at forces between 56 and 66 % of the estimated bending resistance, close to what is calculated for RC slab PG20. The composite slabs with only a 25-mm layer of UHPFRC (SAMD2 and PBM2) reached a higher ratio of their respective bending resistance, between 72 and 85 % of V_{flex}, which is similar to what is observed for the reference RC slab PG19.

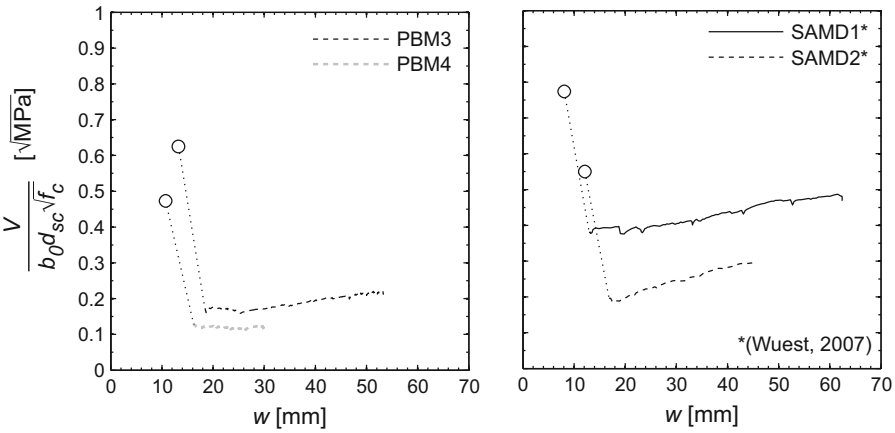

Fig. 11 Post-peak behaviour of selected slabs as a function of the normalized force

Table 4 Comparison of the test results to resistance models for RC slabs

Slab	V_R (kN)	ψ_R (‰)	V_{flex} (kN)	V_R/V_{flex} (–)	V_{csct} (kN)	V_R/V_{csct} (–)	ψ_{csct} (‰)
SAMD1[b]	971	9.6[a]	1597	0.61	454	2.14	16.1
SAMD2[b]	675	13.4[a]	798	0.85	448	1.51	16.6
PBM1	1089	11.9	1654	0.66	644	1.69	11.3
PBM2	1223	12.2	1948	0.63	701	1.74	12.7
PBM3	1186	11.3	2099	0.56	662	1.79	12.8
PBM4	1023	9.1	1417	0.72	771	1.33	11.0
PG19[c]	860	12.1	1196	0.72	805	1.07	12.4
PG20[c]	1094	9.2	2225	0.49	1076	1.02	7.3

[a] Calculated

[b] Tested by Wuest [19]

[c] Tested by Guidotti [20]

5.3 Critical shear crack theory

The resistance to punching shear of the RC section of each composite slab was estimated using the CSCT proposed by Muttoni [10]. As seen in Table 4, for a 50-mm UHPFRC layer, the resistance of the composite slabs was at least 69 % higher than the calculated resistance of the RC section alone using the following analytical expression [10]:

$$\frac{V_{csct}}{b_0 d_{sc}\sqrt{f_c}} = \frac{3/4}{1 + 15\frac{\psi_{csct} d_{sc}}{d_{g0}+d_g}} \quad (4)$$

Since the layers of UHPFRC are kept thin relatively to the concrete thickness, it can be supposed that a major part of the shear stress is carried by the RC section, as proposed by Noshiravani and Brühwiler [7] for composite beams. The punching resistance of the RC section depends on its deformation which can be measured by its rotation, as proposed by the CSCT. The layer of UHPFRC, as was shown, helps to increase the deformation in the RC section.

Existing models to calculate the punching resistance of a RC slab that account for the deformation of the slab, such as the CSCT, can thus be used to predict the concrete contribution to the resistance of a composite slab. The failure criterion as proposed by the CSCT is plotted with the force—rotation curves, in Fig. 4. It intersects the curves at forces over 75 % and over 90 % of V_R for a 50-mm and 25-mm layer of UHPFRC respectively. The resistance beyond the criterion is due to the contribution of the UHPFRC.

6 Conclusion

The following conclusions can be drawn on the basis of the experimental investigation presented herein:

(1) The layer of UHPFRC increases the normalized punching resistance of the RC section by at least 69 % for a layer of 50 mm. At maximum resistance, the rotation capacity of the composite slab is comparable to that of the reference RC slab.

(2) The use of reinforcement in the UHPFRC layer does not have an important influence on the resistance or deformation of the composite slab because punching failure happens before yielding of the reinforcement. Yet, it could significantly make a difference in the bending resistance and should be considered in the design of composite sections [5].

(3) The layer of UHPFRC provides shear resistance to the cracked RC section by out of plane bending. At the mouth of the critical shear crack, bending efforts are introduced in the layer due to the relative movement of the lips of the crack. Over the column, the layer deflects upward due to these bending efforts. Because of geometrical compatibility, limited horizontal cracking is created in the concrete underneath the interface.

(4) The layer of UHPFRC increases the rigidity of the slab, as an added flexural reinforcement is expected to do. However, the deformability of UHPFRC in bending allows the RC section to deform. Shear deformation and crack opening of the RC section are larger than for the reference RC slab. This results in rotations and deflections at maximum resistance similar to what is observed for the reference RC slab.

(5) A thinner UHPFRC layer of 25 mm also increases the punching resistance and rigidity of a slab. However, this thinner layer evidently has less bending resistance than a layer of 50 mm and the rotation at maximum resistance is smaller than for the reference RC slab.

(6) The CSCT model for RC slabs cannot be used to directly calculate the maximum resistance and deformability of composite slabs. This model may be used to determine the contribution of the RC section of the composite slabs and a new term has to be developed to account for the contribution of the UHPFRC layer.

Acknowledgments The authors would like to acknowledge Holcim Switzerland for donating the UHPFRC premix S3-13 used to fabricate slab series PBM.

References

1. Broms CE (2000) Elimination of flat plate punching failure mode. ACI Struct J 97(1):94–101
2. Habel K, Denarié E, Brühwiler E (2006) Structural response of elements combining ultrahigh-performance fiber-reinforced concretes and reinforced concrete. J Struct Eng 13(11):1793–1800
3. Denarié E, Brühwiler E (2011) Strain hardening of ultra-high performance fibre reinforced concrete: deformability versus strength optimization. Int J Restor Build Monum 12(6):397–410
4. Brühwiler E, Denarié E (2013) Rehabilitation and strengthening of concrete structures using ultra-high performance fiber reinforced concrete. Struct Eng Int 23(4):450–457
5. Oesterlee C (2010) Structural response of reinforced UHPFRC and RC composite members. Dissertation, EPFL, Lausanne
6. Habel K, Denarié E, Brühwiler E (2007) Experimental investigation of composite ultra-high-performance fiber reinforced concrete and conventional concrete members. ACI Struct J 104(1):93–101
7. Noshiravani T, Brühwiler E (2013) Experimental investigation on R-UHPFRC–RC composite beams subjected to combined bending and shear. ACI Struct J 110(2):251–261
8. Bastien-Masse M (2014) Punching test on R-UHPFRC–RC composite slabs without shear reinforcement. Test report. MCS, EPFL, Lausanne
9. Guandalini S, Burdet OL, Muttoni A (2009) Punching tests of slabs with low reinforcement ratios. ACI Struct J 106(1):87–95
10. Muttoni A (2008) Punching strength of reinforced concrete slabs without transverse reinforcement. ACI Struct J 105(4):440–450
11. Theodorakopoulos DD, Swamy RN (2002) Ultimate punching shear strength analysis of slab-column connections. Cem Concr Compos 24:509–521
12. Menétrey Ph (2002) Synthesis of punching failure in reinforced concrete. Cem Concr Compos 24:497–507
13. Koppitz R, Kenel A, Keller T (2013) Punching shear of RC flat slabs—review of analytical models for new and strengthening of existing slabs. Eng Struct 52:123–130
14. Amsler M, Thoma K, Heinzmann D (2014) Punching slab strengthened with an additional concrete layer—test and recalculations. Beton- und Stahlbetonbau 109(6):394–402
15. Chen C-C, Li C-Y (2005) Punching shear strength of reinforced concrete slabs strengthened with glass fiber-reinforced polymer laminates. ACI Struct J 102(4):535–542
16. Esfahani MR, Kianoush MR, Moradi AR (2009) Punching shear strength of interior slab-column connections strengthened with carbon fiber reinforced polymer sheets. Eng Struct 31:1535–1542
17. Harajli MH, Soudki KA (2003) Shear strengthening of interior slab-column connections using fiber-reinforced polymer sheets. J Compos Constr 7(2):145–153
18. Sharaf MH, Soudki KA, Van Dusen M (2006) CFRP strengthening for punching shear of interior slab-column connections. J Compos Constr 10(5):410–418
19. Wuest J (2007) Comportement structural des bétons de fibres ultra performants en traction dans des éléments composés. Dissertation, EPFL, Lausanne
20. Guidotti R (2010) Poinçonnement des planchers-dalles avec colonnes superposées fortement sollicitées, Dissertation, EPFL, Lausanne

21. Clément T, Pinho Ramos A, Fernández Ruiz M, Muttoni A (2014) Influence of prestressing on the punching strength of post-tensionned slabs. Eng Struct 72:59–69
22. Lips S, Fernandez Ruiz M, Muttoni A (2012) Experimental investigation on punching strength and deformation capacity of shear-reinforced slabs. ACI Struct J 109(6):889–900
23. Rossi P (1997) High performance multimodal fiber reinforced cement composites (HPMFRCC): the LCPC experience. ACI Mater J 94(6):478–483
24. Rossi P, Arca A, Parant E, Fakhri P (2005) Bending and compressive behaviors of a new cement composite. Cem Concr Res 35:27–33
25. Fernández Ruiz M, Mirzaei Y, Muttoni A (2013) Post-punching behavior of flat slabs. ACI Struct J 110(5):801–811
26. Habibi F, Cook WD, Mitchell D (2014) Predicting post-punching shear response of slab-column connections. ACI Struct J 111(1):123–134